

# Pre-Main Sequence stars in the star forming complex Sh 2-284\*

F. Cusano<sup>1†</sup>, V. Ripepi<sup>1</sup>, J. M. Alcalá<sup>1</sup>, D. Gandolfi<sup>2</sup>, M. Marconi<sup>1</sup>, S. Degl’Innocenti<sup>3,4</sup>, F. Palla<sup>5</sup>, E. W. Guenther<sup>6</sup>, S. Bernabei<sup>7</sup>, E. Covino<sup>1</sup>, C. Neiner<sup>8</sup>, E. Puga<sup>9,10</sup>, S. Hony<sup>11</sup>

<sup>1</sup> *INAF-Osservatorio Astronomico di Capodimonte, Salita Moiariello16, 80131 - Napoli, Italy*

<sup>2</sup> *Research and Scientific Support Department, ESTEC/ESA, PO Box 299, 2200 AG Noordwijk, The Netherlands*

<sup>3</sup> *Dipartimento di Fisica, Università di Pisa, Largo B. Pontecorvo 3, 56126 Pisa, Italy*

<sup>4</sup> *INFN, Sezione di Pisa, Largo B. Pontecorvo 3, 56126 Pisa, Italy*

<sup>5</sup> *INAF-Osservatorio Astrofisico di Arcetri, Largo E. Fermi, 5, I-50125, Firenze, Italy*

<sup>6</sup> *Thüringer Landessternwarte Tautenburg, Sternwarte 5, D - 07778, Tautenburg, Germany*

<sup>7</sup> *INAF-Osservatorio Astronomico di Bologna, Via Ranzani 1, 40127 Bologna, Italy*

<sup>8</sup> *GEPI, UMR 8111 du CNRS, 5 place Jules Janssen, 92195 Meudon Cedex, France*

<sup>9</sup> *Katholieke Universiteit Leuven, Celestijnenlaan 200D, 3001 Leuven, Belgium*

<sup>10</sup> *Centro de Astrobiología (CSIC-INTA), Ctra. de Torrejón km-4, E28850, Torrejón de Ardoz, Madrid, Spain*

<sup>11</sup> *CEA Saclay, Bat.609 Orme des Merisiers, 91191 Gif-sur-Yvette, France*

Accepted . Received

## ABSTRACT

Located at the galactic anticenter, Sh 2-284 is a HII region which harbors several young open clusters; Dolidze 25, a rare metal poor ( $Z \sim 0.004$ ) young cluster, is one of these. Given its association with Sh 2-284, it is reasonable to assume the low metallicity for the whole HII region. Sh 2-284 is expected to host a significant population of Pre-Main Sequence (PMS) stars of both low and intermediate mass stars (Herbig Ae stars). We aim at characterizing these stars by means of a spectroscopic and photometric survey conducted with VIMOS@VLT and complemented with additional optical and infrared observations. In this survey we selected and characterized 23 PMS objects. We derived the effective temperature, the spectral energy distribution and luminosity of these objects; using theoretical PMS evolutionary tracks, with the appropriate metallicity, we estimated the mass and the age of the studied objects. We also estimated a distance of 4 Kpc for Sh 2-284 by using spectroscopic parallax of 3 OB stars. From the age determination we concluded that triggered star formation is in act in this region. Our results show that a significant fraction of the young stellar objects (YSOs) may have preserved their disk/envelopes, in contrast with what is found in other recent studies of low-metallicity star forming regions in the Galaxy. Finally, among the 23 bona fide PMS stars, we identified 8 stars which are good candidates to pulsators of the  $\delta$  Scuti type.

**Key words:** stars: pre-main sequence, stars: formation, open clusters and associations: individual: Sh 2-284, stars: variables: T Tauri, Herbig Ae/Be .

## 1 INTRODUCTION

Dolidze 25 is a young (age  $\approx 6$  Myr; Turbide & Moffat 1993) open cluster associated with the HII region Sh 2-284 (Sharpless 1959) located in the galactic anticenter. On

the basis of high-resolution spectroscopy of three OB stars, Lennon et al. (1990) estimated that Dolidze 25 is deficient in metals by a factor of about 6 with respect to the Sun. This result was confirmed later by Fitzsimmons et al. (1992). Dolidze 25 hence represents a very rare case of galactic low-metallicity young cluster. The association of Dolidze 25 to Sh 2-284, leads to the conclusion that the HII region and the star forming sites in Sh 2-284 are characterized by a low metallicity. Delgado et al. (2010) proposed the presence of two populations of stars in Dolidze 25. One composed by

\* Based on observations carried out at the European Southern Observatory (Paranal, Chile) under programme No. 074.C-0111. and partly at the Anglo-Australian Telescope in program 07B/040 and 08B/003.

† E-mail: fcusano@na.astro.it

young stars of 3-4 Myr and the other one by older stars with an average age of 40 Myr. The average cluster reddening derived by Delgado et al. (2010) is  $E(B-V)=0.78$ , which is in good agreement with the value  $E(B-V)=0.81 \pm 0.11$  estimated by Moffat & Vogt (1975).

It is well known that a great part of YSOs (Class I and Class II objects; see Lada et al. 1987) show infrared excess, which is interpreted in terms of the presence of a circumstellar disk/envelope. Infrared colour-colour (CC) and colour-magnitude (CM) diagrams are good diagnostic tools for the investigation of circumstellar matter around YSOs (Hartmann et al. 2005; Lada et al. 2006; Harvey et al. 2007; Alcalá et al. 2008, and references therein). Recently, Puga et al. (2009, hereafter P09) carried out an infrared photometric survey of the star forming region in Sh 2-284, using the Infrared Array Camera (IRAC; Fazio et al. 2004) on board the Spitzer Space Telescope (Werner et al. 2004). Based on the [3.6]-[4.5] vs. [5.8]-[8.0] diagram P09 selected 338 candidates to infrared-excess YSOs. They classified 155 and 183 as Class I and Class II IR sources, respectively and studied their spatial distribution. They found that the YSO candidates concentrate in several aggregates, one of which is projected on the field of Dolidze 25. They conclude that triggered star formation may be at work in the region. Both the works by P09 and Delgado et al., do provide a photometric characterization of the sources, but no spectroscopic information on the low and intermediate mass YSOs in Sh 2-284 and members of Dolidze 25 is available.

In this paper we present the results of a photometric and spectroscopic follow-up of Sh 2-284 using VIMOS (Visual & Multi-Object Spectrograph, LeFevre et al. 2003) at VLT. We aim at characterizing low and intermediate mass PMS stars of the region to study star formation in such low-metallicity environment. Our interest is also focused on the identification of intermediate-mass ( $1.5M_{\odot} \leq M \leq 4M_{\odot}$ ) PMS stars falling in the  $\delta$ -Scuti instability strip (Breger 1972). Since about ten years it is known that such stars, during their contraction towards the main sequence, cross the instability strip for more evolved  $\delta$ -Scuti stars (Breger & Pamyatnykh 1998). These PMS stars are thus subjected to stellar pulsation (see Marconi & Palla 1998). Therefore, their asteroseismological properties allow to put constraints on the PMS physical parameters such as luminosity, mass and effective temperature, as well as on the internal structure, which is different from that of more evolved stars of the same mass. Good examples of known PMS  $\delta$  Scuti stars are the spectroscopic binary system RS Chamaeleontis (Böhm et al. 2009), V351 Ori (Ripepi et al. 2003) and IP Per (Ripepi et al. 2006). However, the asteroseismological study of some of the  $\delta$  Scuti PMS found here is still in progress and is deferred to another paper (Ripepi et al. 2010, in preparation).

The paper is organized as follows. In Sect. 2 we present our observations and describe the data reduction. In Sect. 3 we discuss the results: the determination of physical parameters together with the selection of bona-fide PMS and their infrared properties. In the same section we give an estimate of the distance of the Sh 2-284 region by using spectroscopic parallax performed on early-type stars. Finally, discussions and conclusions are presented in the Sect. 4 and 5.

## 2 OBSERVATIONS AND DATA REDUCTION

Both photometry and spectroscopy were obtained in service mode with VIMOS at the UT3 of the VLT complex at Paranal (Chile). In the field of Sh 2-284 we obtained photometric data on the 7th October 2005 in the  $R$  and  $I$  filters, for a total of 16 images. The spectroscopic data were acquired the 4th February 2006 and consist of about 1500 spectra at low and medium resolution. In the following subsections we describe the details of the observations and the data reduction.

### 2.1 Photometry

The VIMOS imager is composed by a mosaic of 4 CCDs with gaps of about 2 arcmin for a total field of view (FOV) of  $18' \times 16'$ . In order to image approximately  $30' \times 30'$ , which cover most of the central part of Sh 2-284 HII region, we performed 2 pairs of  $R$  and  $I$  frames with pointings shifted by about 6 arcmin between one pair and the other. Equal exposures of 60 s were performed in both filters.

The images were processed following standard techniques (bias subtraction and flat-field correction) using the IRAF<sup>1</sup> package. The fringing in the  $I$ -band images was corrected by adopting a well-suited fringing map kindly provided to us by E. Held and S. Berta and following the recipe by Alcalá et al. (2002). The images were then astrometrically calibrated using the standard IRAF procedures and the USNO-A2.0 as reference catalogue. The resulting astrometric accuracy is of the order of 0.35 arc-sec RMS.

PSF photometry was performed with the DaophotII/Allstar packages (Stetson 1987, 1992). The photometric calibration was executed by using the standard fields L98 and L110 (Landolt 1992). For this purpose we used the extended list of standards provided by P.B. Stetson<sup>2</sup>, which are sufficiently large in number of stars to include a significant number of objects (>100) in each CCD, allowing the determination of a colour equation independently for all the chips. As a result of this procedure, we obtained four linear and four quadratic calibration equations in the  $R$  and  $I$  bands, respectively. The typical error of the transformations is of the order of 0.01-0.02 mag. We then applied these transformations to the instrumental magnitudes of the objects extracted from our scientific images, and derived the magnitudes in the standard Johnson-Cousins system.

Our photometric catalog was complemented with measurements in other bands from literature. We used: 1)  $BV$  photometry of the same field provided by the COROT EXODAT group (Meunier et al. 2009); 2) the  $JHK$  photometry from the 2-Micron All-Sky Survey (2MASS) point-source catalog (Cutri et al. 2003); 3) the mid-infrared Spitzer photometry at 3.6, 4.5, 5.8, and 8  $\mu\text{m}$ , obtained under the program 3340 (P09). As result, we end up with a photometric catalogue with a large wavelength coverage, from the optical to the mid-infrared, which is crucial to investigate the PMS

<sup>1</sup> IRAF is distributed by the National Optical Astronomical Observatories, which are operated by the Association of Universities for Research in Astronomy, Inc., under cooperative agreement with the National Science Foundation

<sup>2</sup> <http://cadwww.dao.nrc.ca/standards/>

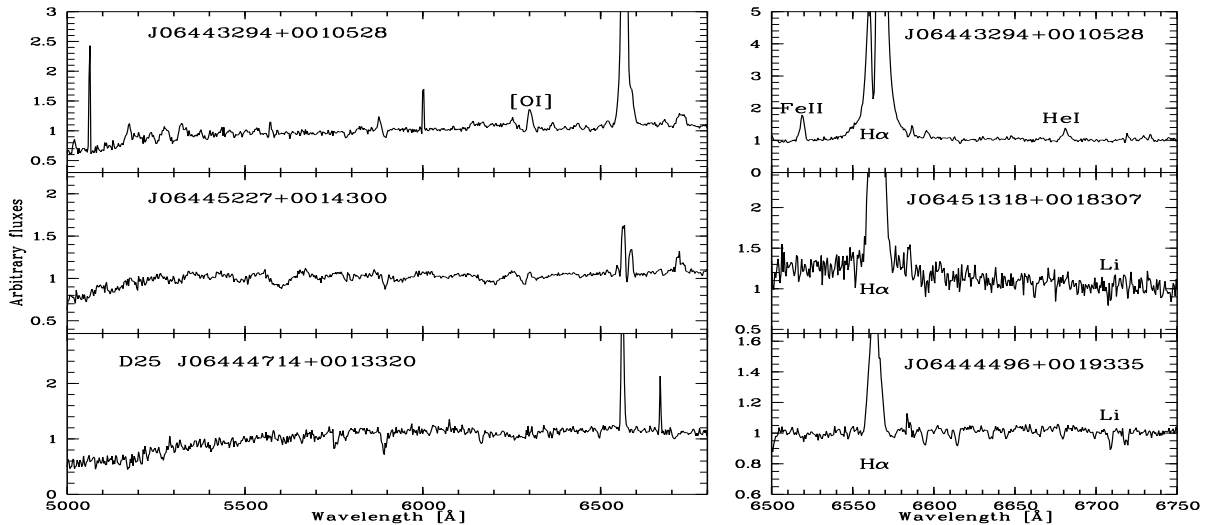


**Figure 1.** The MR spectra of three PMS stars in Sh 2-284 are shown in the left panels. The right panels show the HR spectra of other PMS stars in the region. The later cover the spectral region between 6500 and 6750 Å, where the H $\alpha$  emission and the lithium absorption lines can be seen. Emission lines due to stellar wind ([OI]) and accretion process (H $\alpha$ ) are well detected in the spectrum of J06443294+0010528.

nature of our sources in terms of infrared excess in their spectral energy distribution.

## 2.2 Spectroscopy

The multi-slit spectroscopy was acquired using the Medium Resolution (MR), High Resolution (HR) Red and the HR Orange<sup>3</sup> grisms. The wavelength coverage and resolution corresponding to these grisms are: 4800-10000 Å with 2.5 Å/pix, 6500-8750 Å with 0.6 Å/pix and 5150-7600 Å with 0.6 Å/pix for MR, HR red and HR orange grisms, respectively. Note, however, that the spectral coverage for each object depends on the position of the corresponding slit relative to the center of the VIMOS quadrants. In each CCD we were able to observe around 40 and 30 objects simultaneously with the MR and HR grisms, respectively. In total, we obtained 912 spectra with the MR red and 594 spectra with the HR Red and Orange grisms. The exposure time was 900 s for the MR grism with an average S/N  $\sim$ 40-50, whereas for the HR grism the exposure time was 2000 s with an average S/N  $\sim$ 20-30.

The bias subtraction, flat field correction, sky subtraction, wavelength calibration of the spectra were performed using the ESO VIMOS automatic pipeline. Subsequent extraction of the spectra was executed using the IRAF routine *apall*. As a test of the goodness of the data reduction performed using the pipeline, we also processed a few spectra by hand using the standard IRAF routines. The comparison of the results showed that the automatic pipeline provides scientifically useful spectra. Unfortunately, the spectral region with  $\lambda > 7000\text{\AA}$  of the low-resolution spectra is useless due to strong fringing. Some examples of spectra are shown in Fig. 1.

<sup>3</sup> The Orange grism was used in quadrant 4 due to the lack of a HR red grism for this CCD

Finally, we calibrated all the spectra in relative flux. To this aim flux standard stars were observed during the same nights as the scientific frames. The standard stars were reduced using IRAF standard routines. A response function was derived for each of the four VIMOS quadrants.

Due to constraints on the software used to prepare the VIMOS masks (VIMOS Mask Preparation Software, VMMP), it was not possible to configure slits on many interesting candidates selected from optical colour-magnitude diagrams, preventing the observation of high-priority targets. However, it was possible to automatically assign slits to other objects in the field of the cluster.

Additional low-resolution spectroscopy of three OB stars was performed in January 2008 with the AAOmega multi-object facility mounted at the AAT-3.9 m telescope of the Anglo-Australian Observatory. Two out of these three stars were investigated by Lennon et al. (1990) and are indicated in this paper as star number 15 and 22. These observations are part of a large spectroscopic follow-up program devoted to the study of the stellar population in the *CoRoT* fields and will be described in detail in a forthcoming paper (Gandolfi et al., in preparation). The *580V* and *385R* low-resolution gratings were used for the blue and red arm of the spectrograph, respectively, yielding a spectral coverage of about 3700 Å (3730 – 7430 Å) with a mean resolving power of  $R \approx 1300$ .

## 3 RESULTS

The spectroscopy in this work represents a step forward with respect to the previous photometric studies of Sh 2-284. Thus, we discuss first the photometric results and then use them to further investigate the photometric properties, from mid-IR to optical, of the YSO candidates in the region.

### 3.1 Spectroscopically identified PMS stars

The main criteria used for the selection of PMS stars are the presence of H $\alpha$  emission plus near and mid IR excess of emission relative to normal stars of the same spectral type. Both processes trace the presence of circumstellar material around YSOs. The H $\alpha$  emission on one side, indicates accretion from the circumstellar disk towards the star. The infrared excess comes indeed from the thermal disk emission. To detect young stars, an additional criterion is the presence in the spectra of the LiI ( $\lambda 6708\text{\AA}$ ) absorption line, for stars with spectral type later than about G5. The Lithium, in fact, is efficiently burned in the first million years of PMS stellar evolution.

#### 3.1.1 H $\alpha$ emission

First, an inspection of all the available spectra was performed searching for H $\alpha$  emission-line stars. This inspection led to the identification of 35 emission-line objects, which are reported in Table 2 and 3 together with the photometric measurements. The equivalent width of the H $\alpha$  line was then measured using IRAF. Such measurements, reported in Table 4 and 5, were performed by Gaussian fitting, defining the continuum by fitting a low order spline to selected spectral regions in both sides of the H $\alpha$  line. The errors in such measurements come mainly from the uncertainty in the continuum definition when selecting the regions near the line. Since the H $\alpha$  criterion alone cannot discriminate between PMS stars and field emission-line stars, we used additional criteria based on the available IR photometry (see Section 3.2).

#### 3.1.2 Spectral types

The spectral typing was performed on the H $\alpha$  emitting-stars by using calibrations in the literature between equivalent width of some spectral lines versus spectral type as follows: i) the blend between Ca I and Fe I at  $5270\text{\AA}$  (Hernández et al. 2004) and ii) the Na I line at  $5892\text{\AA}$  (only for spectral type later than K0 Tripicchio et al. 1997). As a check of the spectral type determinations we have also performed a  $\chi^2$  minimization of a grid of spectral templates on the available spectra of the PMS candidates. This procedure is similar to the one described in Frasca et al. (2003). The derived spectral types are reported in Tab. 4 and 5 together with the equivalent width of the CaI+FeI blend and the NaI line. The average uncertainty on spectral classification is estimated to be of one and two subclasses for high and low S/N spectra, respectively. The spectral type was used to derive the individual reddening and spectral energy distribution (SED) of the PMS stars (See Section 3.3).

#### 3.1.3 Lithium absorption

The presence of LiI ( $\lambda 6708\text{\AA}$ ) absorption feature in the spectrum of late-type stars, can be used as an additional check for the PMS nature of the stars. In the low-resolution spectra the line is blended with neutral iron lines. Thus, the line should be sought in the available VIMOS high-resolution spectra. Among the stars selected above, only 10 have high-resolution VIMOS spectra, but only five have sufficient S/N

to detect the LiI line. We unambiguously detect the line in all of them. Examples are shown in Fig. 1, adding support to our selection criteria.

#### 3.1.4 Vetted PMS stars

On the basis of the above arguments 23 bona-fide PMS objects were identified. One of these, namely J06450075+0013356, was rejected as PMS star by Delgado et al. (2010), but our medium resolution spectrum ( $R \sim 2500$ ) shows strong H $\alpha$  emission and lithium absorption (see Table 4). In addition, its SED shows infrared excess (See section 3.3 and Figure 7). The 23 PMS stars are listed in Table 4.

Other two objects that show H $\alpha$  emission, namely J06453567+0018473 and J06451118+0011402, match fairly well the age of PMS stars in the field of Dolidze 25 when assuming the distance of 4.0 Kpc (see Section 3.1.5). However, since we lack their medium resolution spectrum, we cannot confirm or reject their PMS nature based on the Li absorption line. We thus refer to these two objects as potential PMS stars.

The remaining 10 H $\alpha$  emission line objects correspond to active field K and M-type stars, unrelated to the star forming region, but we also provide their coordinates and photometry in Table 3 and the spectral types in Table 5.

11 of the 23 PMS stars coincide with YSO candidates by P09, which means that their selection missed about half of the PMS stars. However, in order to be able to apply the selection criterion adopted by P09, it is necessary that the sources are detected in all four IRAC bands. Note that 6 of the PMS stars were not detected in at least one IRAC band, while other 6 have mid-IR colours typical of Class III sources. The latter is further discussed in Section 3.2.

#### 3.1.5 On the distance of Sh 2-284

There has been controversy on the heliocentric distance determinations of Sh 2-284. Lennon et al. (1990) and Turbide & Moffat (1993) give an estimate of  $\sim 6$  Kpc. Russeil, Adami & Georgelin (2007) determined a distance of  $6.03 \pm 1.16$  Kpc. They claim that Sh 2-284 belongs to a broader complex at  $7.89 \pm 0.27$  Kpc, which also includes the HII regions Sh 2-283, 285 and 286 (Sharpless 1959). A spectrophotometric distance of  $5.2 \pm 0.8$  Kpc for Sh 2-284 was also determined by Avedisova & Kondratenko (1984). However, all these studies did not account for the low-metallicity. More recently, Delgado et al. (2010) estimated a distance of 3.6 Kpc by using low-metallicity isochronal fitting on *UBV* CM diagrams of Dolidze 25, but they claim that the distance could be as high as 4 Kpc when considering systematic effects on metallicity determinations. In order to further investigate the distance of the Sh 2-284 region, we performed a detailed analysis of three early-type stars in the field of Dolidze 25. These stars are 2MASSJ06450217+0013294, 2MASSJ06451043+0011164, and 2MASSJ06441748+0020315. The first two stars are also identified as star number 15 and 22 by Moffat & Vogt (1975), respectively. The spectral type and luminosity class of the target stars were derived by fitting the AAOmega spectra with a suitable grid of observed stellar templates (see example Figure 2), as described in

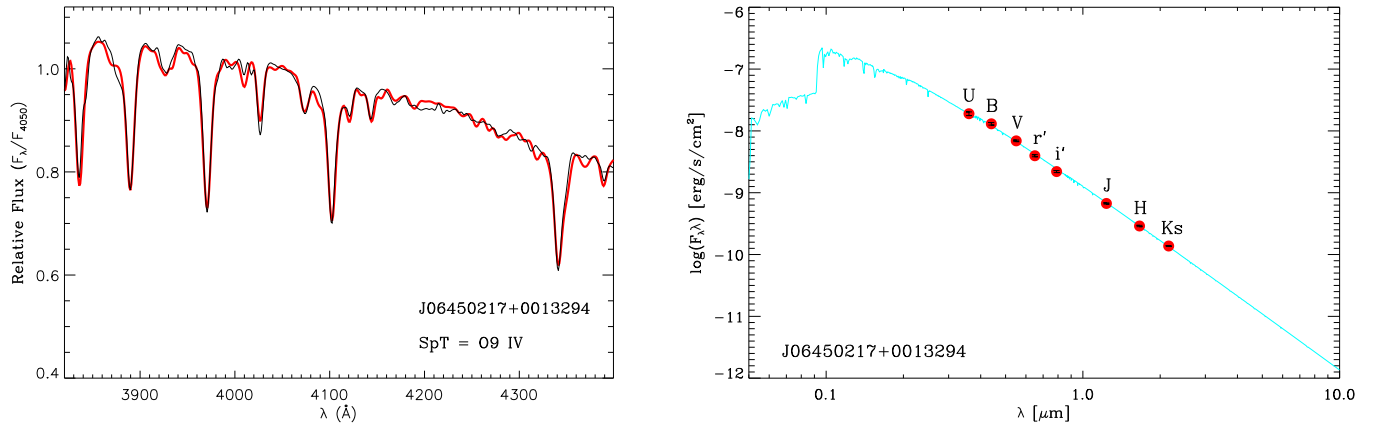


**Figure 2.** Left: AAOmega spectrum of J06450217+0013294 (thin black line). The best fitting O9 IV template is over-plotted with a thick red line. The spectra were normalised to the flux at 4050 Å. Right: SED of J06450217+0013294. The red filled dots mark the dereddened optical and near-infrared fluxes. The model spectrum from Kurucz (1979), with the same effective temperature as the star, is over-plotted with a light blue thin line.

**Table 1.** Physical parameters of the stars used to determine the distance of Sh 2-284. The fifth column reports the observed V-magnitude taken from the EXO-DAT (Meunier et al. 2009).

id (2MASS)	id <sup>1</sup>	$\alpha$ (J2000)	$\delta$ (J2000)	V [mag]	SpT	$T_{\text{eff}}$ [K]	$M_V$ [mag]	$A_V$ [mag]	$R_V$	$d^*$ [pc]
J06450217+0013294	15	06 45 02.18	00 13 29.5	11.66	O9 IV	33 000	$-4.9 \pm 0.2$	$2.92 \pm 0.03$	$3.30 \pm 0.05$	$4060 \pm 500$
J06451043+0011164	22	06 45 10.44	00 11 16.4	12.07	B1 IV	25 000	$-3.9 \pm 0.2$	$2.27 \pm 0.08$	$3.20 \pm 0.20$	$4172 \pm 500$
J06441748+0020315		06 44 17.49	00 20 31.5	11.93	B0e IV	31 000	$-4.4 \pm 0.2$	$2.60 \pm 0.10$	$3.60 \pm 0.20$	$4197 \pm 500$

<sup>1</sup> from Moffat & Vogt (1975)

\*: distance estimated by adding 0.6 mag to  $M_V$  as a correction due to low-metallicity.

Frasca et al. (2003) and Gandolfi et al. (2008). The effective temperature ( $T_{\text{eff}}$ ) and absolute magnitude ( $M_V$ ) of each star was assigned using tabulated scales from the compilation of Straižys & Kuriliene (1981). A good agreement was found between the adopted  $M_V$  values and the absolute magnitudes derived using the empirical  $H_\gamma$ - $M_V$  calibration from Millward & Walker (1985). We constructed the spectral energy distribution (SED) of the target stars (Figure 2) by merging the EXO-DAT  $BVr'i'$  broad-band photometry (Meunier et al. 2009) with the U-magnitudes from Moffat & Vogt (1975) and the  $JHKs$  near-infrared photometry from the 2MASS catalogue. Following the two-parameter method described in Gandolfi et al. (2008), we derived the interstellar extinction ( $A_V$ ) and the total-to-selective extinction  $R_V=A_V/E_{B-V}$  by fitting simultaneously the observed colors encompassed by the SED with synthetic colors computed using Kurucz 1979's atmosphere models with the same spectral type and luminosity class as the stars. The low-metallicity is taken into account by applying a correction to the absolute magnitude, appropriate for the metallicity of the region. Such correction, on the order of 0.6 mag, was determined using the relationship by Vandenberg & Poll (1989) and adopting  $[\text{Fe}/\text{H}]=-0.55$ . We checked that this correction

is valid for the range of intrinsic colors of the three stars by using the isochronal tools described by Marigo et al. (2008). Finally, the individual distance to the stars was estimated using the metallicity-corrected  $M_V$  and  $A_V$  values, as well as the observed EXO-DAT V-magnitude. The derived physical parameters of the target stars are listed in Table 1. The estimated average distance of 4 Kpc, is in agreement with the upper value claimed by Delgado et al. (2010). Such distance places Dolidze 25 at a galactocentric distance of 12 Kpc. These values of galactocentric distance and metallicity are also consistent with the relationship between metallicity versus galactocentric distance for open clusters observed by Sestito et al. (2008). Thus, we adopt a heliocentric distance of 4 Kpc for subsequent analysis in this paper.

## 3.2 Photometric properties

### 3.2.1 Mid-IR colour-magnitude and colour-colour diagrams

The classification of the sources as Class I and Class II YSOs by P09 was based solely on the  $[3.6]-[4.5]$  vs.  $[5.8]-[8.0]$  diagram, but other combinations of colours and magnitudes

can be used to check the selection and classification, by also incorporating the near-IR 2MASS data. The two upper panels of Fig. 3 show the Spitzer CM diagrams of all the sources detected in Sh 2-284, while the lower panels show the near-mid IR CC diagrams of those sources with 2MASS data. Most of the YSO candidates selected by P09 satisfy the “cores-to-disk” (c2d; Evans et al. 2003, 2009) criterion for the selection of YSO candidates based on IRAC-only data (e.g. Porras et al. 2007), but some might be extragalactic contaminants, in particular several Class I candidates that fall below the inclined dashed line in the [8.0] vs. [4.5]-[8.0] CM diagram. The Class I and Class II sources are well distinguished in the Spitzer CM diagrams, while most of the spectroscopically identified PMS stars have typical colours of Class II and Class III sources. In particular, six of the latter can be well distinguished in the [4.5] vs. [3.6]-[4.5] CM diagram, typically at [3.6]-[4.5] colours below 0.4 mag. Note also that the potential PMS stars have colours of Class III sources. These two objects remained undetected at 8 micron.

Not all the the sources detected by Spitzer in the Sh2-284 region were also detected by the 2MASS. The objects matching the two catalogues are plotted in the CC diagrams shown in the low panel of Fig. 3. The stars with normal photospheric colours, all basically at zero, are well distinguished from the YSOs, but as noted above several of the spectroscopically identified PMS stars possess normal photospheric colours. These objects represent part of the diskless PMS population of Sh 2-284.

### 3.2.2 Near-IR colour-colour diagram

Near IR colours are useful to select objects with optically thick disks, typical of Classical T Tauri stars. Fig. 4 shows near-IR CC diagrams for the PMS stars and for all the IRAC sources that possess 2MASS  $J$ ,  $H$ , and  $K$  measurements. Most of the Class I and Class II YSO candidates by P09, overplotted on the left panel of Fig. 4, have near-IR colours consistent with reddened YSOs, but several are scattered towards bluer ( $J - H$ ) colours and fall below the locus for classical T Tauri stars (Meyer, Calvet & Hillenbrand 1997), in a region consistent with colours of Herbig Ae stars. Likewise, many of the PMS stars have colours consistent with those of classical T Tauri stars, but several lie below that locus as well.

Hernández et al. (2005) proposed a criterion to identify candidates to Herbig AeBe stars on the *intrinsic* near-IR CC diagram. Such diagram for the PMS stars in Sh 2-284 is shown in the right panel of Fig. 4. The field  $H\alpha$  emission stars are also plotted for comparison. The figure also shows the approximate locus corresponding to intermediate-mass PMS stars (see e.g. Hernández et al. 2005). The intrinsic colours were derived using the spectral types (see Section 3.3). Seven PMS stars satisfy the criterion by Hernández et al. (2005).

Finally, we notice that a few YSO candidates by P09 have near-IR colours similar to those of giants. Recent works (e.g. Oliveira et al. 2007) have pointed out the possible contamination by giants among the samples of IRAC-selected YSO candidates.

### 3.2.3 Optical colour-magnitude diagrams

The  $R$  and  $I$  bands are less affected by the continuum dust emission from the YSO disk. Corrected by interstellar extinction, these bands are suitable to prove the continuum stellar photospheric contribution. Therefore, optical colour-magnitude diagrams can be used to trace the stellar sequence of the different aggregates in Sh 2-284. The VIMOS observations cover an area of  $\sim 900$  square-arcmin that include four of the aggregates studied by P09, namely Dolidze 25, Cl2, RN and RW. From our optical catalog we extracted sources on these regions, with approximately the same projected sky area ( $\sim 40$  arcmin<sup>2</sup>) as analysed by P09. Fig. 5 shows the observed  $I$  vs.  $R - I$  diagrams for each one of the four regions. The diagrams show also the 1, 2 and 20 Myr isochrones with metallicity  $Z=0.004$  (solid line, Tognelli et al. 2010). The spectroscopically selected PMS stars and the YSO candidates by P09 in these regions are also overplotted with the same symbols as in Fig. 3.

The average extinction, derived from the spectral type of the PMS stars (See Section 3.3), is approximately the same in the four regions. The 1, 2 and 20 Myr isochrones shown in Fig. 5 were reddened by such average value of  $A_V \sim 2.6$  mag. The magnitudes of the isochrones were also corrected by the distance modulus of Sh 2-284 (13.0 mag).

Most of the PMS stars and YSO candidates are consistent with ages of the order of 1-2 Myr, but some are scattered towards younger or older ages. In particular, the PMS stars and YSO candidates are more scattered in the diagrams of RN and Cl2 regions than in the diagrams of Dolidze 25 and RW. This may indicate that the objects in Dolidze 25 and RW are younger than those in RN and Cl2, in agreement with the findings by P09. They concluded that the YSO candidates projected on Dolidze 25 are younger, in relative terms, than those in the other aggregates. This result is further discussed in Section 3.5.

### 3.2.4 IR colours versus $H\alpha$ emission

Previous works (Hartmann et al. 1998; Lada et al. 2006) shown that stars with strong  $H\alpha$  emission in Taurus and IC 348 tend to possess large ( $K - L$ ) excess. The relationship between IR colours and  $H\alpha$  equivalent width,  $EW_{H\alpha}$ , for the PMS stars in Sh 2-284 is shown in Figure 6. Most have IR colours above the minimum for PMS stars with optically thick disks (i.e.  $K - [4.5] > 0.5$  and  $[3.6] - [4.5] > 0.3$  mag, respectively) according to the models by Robitaille et al. (2006). Most of these objects, likely having optically thick disks, also possess  $EW_{H\alpha}$  above the approximate limit for accretion (i.e.  $10 \text{ \AA}$ ). On the other hand, most objects with no prominent  $H\alpha$  emission have small IR colours. Thus, consistently with the results of previous works, the IR colour index of the PMS stars in Sh 2-284 can be also used as diagnostic for accretion. However, the colour indices can be used as overall indicators, but cannot replace detailed measurements of accretion for individual objects.

## 3.3 Spectral Energy Distributions

The characterization of the PMS stars and their circumstellar matter is performed also through the analysis of the SED (Lada et al. 2006). In order to derive the de-reddened

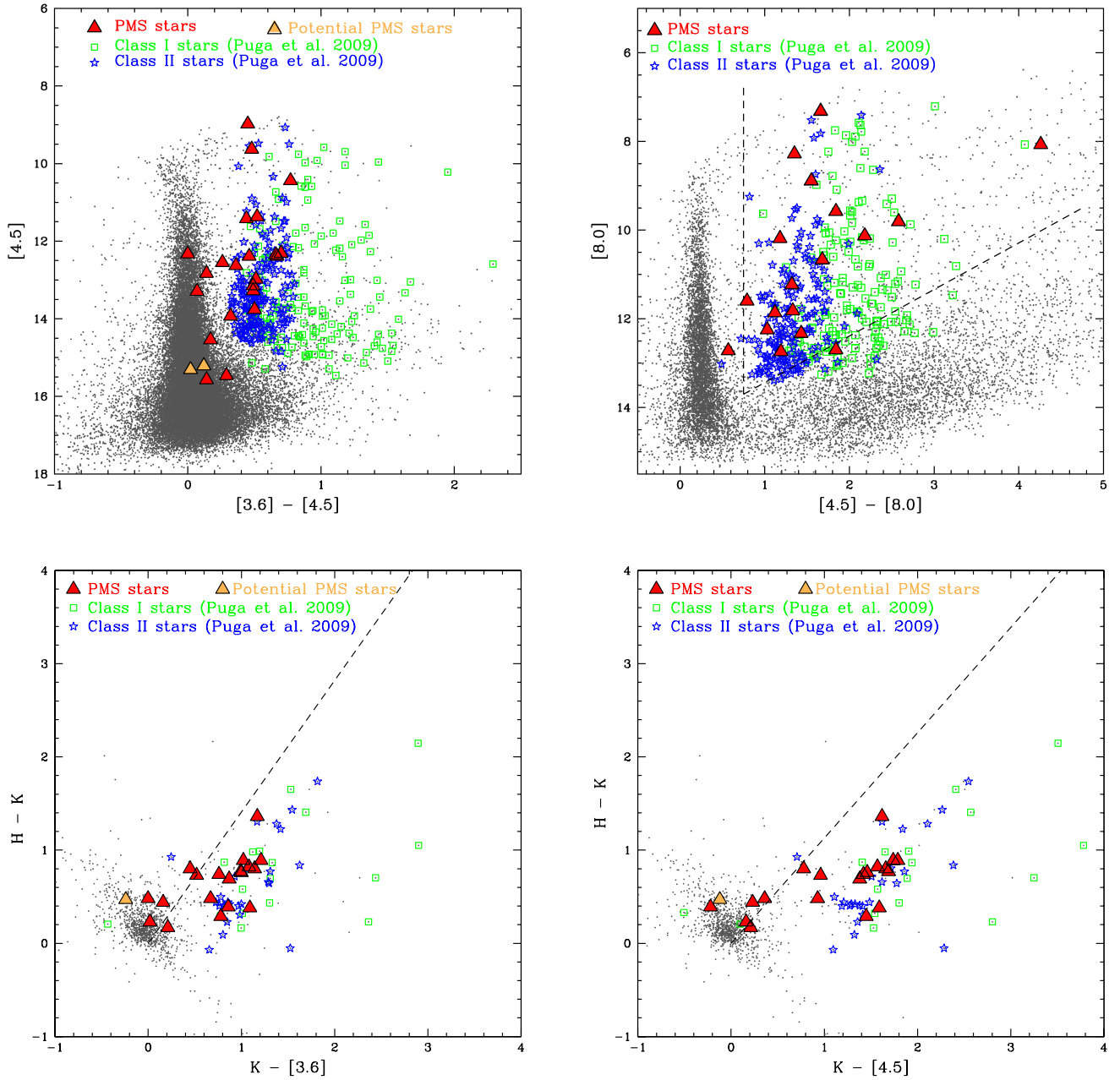


**Figure 3.** IR colour-magnitude and colour-colour diagrams of the sources detected with Spitzer in Sh 2-284 (gray dots). The Class I and Class II YSOs selected by P09 are colour-coded as in the labels. The PMS stars spectroscopically detected in this work (See Section 3.1) are overplotted as red triangles. The criterion adopted by the c2d survey (Evans et al. 2003, 2009) for the selection of candidates to YSOs, based on IRAC-only data (e.g. Porras et al. 2007), is represented with the dashed lines in the  $[8.0]$  vs.  $[4.5]$ - $[8.0]$  CM diagram. The slope of the dashed line in the 2MASS-Spitzer CC diagrams corresponds to the colour-excess ratio by Flaherty et al. (2007).

SEDs it is necessary to use all the available information from the multi-band photometry and spectroscopy. The following steps were adopted to determine the SEDs:

- from the spectral types the effective temperature  $T_{\text{eff}}$  and the intrinsic colour  $(V-I)_0$  of the stars were derived by using the conversion tables of Kenyon & Hartmann (1995).
- the reddening  $E(V - I)$  and the absorption in the  $V$  band,  $A_v$ , were derived comparing the observed  $V - I$

colour, with  $(V-I)_0$ , and assuming  $A_v/E(V - I) = 1.92$  (Cardelli et al. 1989). The  $R - I$  color was used where the  $V$  magnitude was not available. Similarly, the absorption in the other bands was calculated. The values of the effective temperature and the visual extinction for each object are reported in Table 4.

- the magnitudes in all bands were de-reddened and converted into fluxes using the fluxes at zero magnitude given by Bessel (1979).

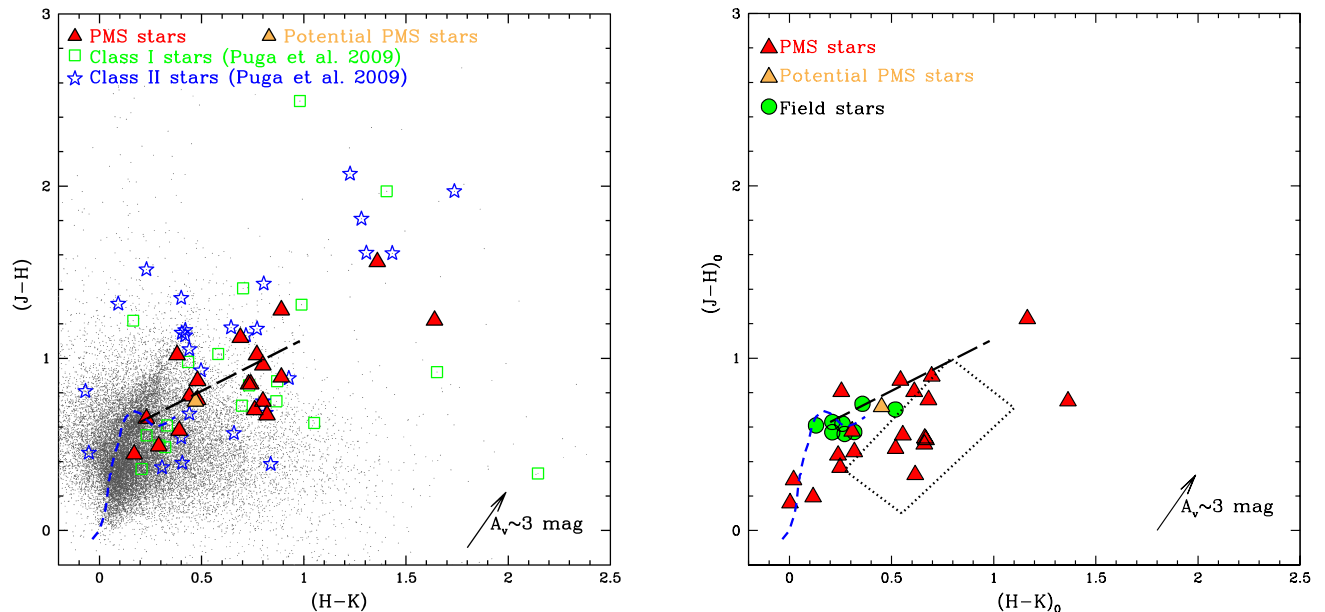


**Figure 4.** Near-IR colour-colour diagrams. *Left:* observed diagram for the identified PMS stars and IRAC sources (grey dots) in Sh 2-284 with  $J$ ,  $H$ , and  $K$  measurements. The Class I and Class II YSO candidates by P09 are overplotted. *Right:* extinction corrected diagram of the PMS stars and  $H\alpha$  emission field stars. Colours were de-reddened using the extinction values reported in the Table 4 and assuming a normal extinction law. The rectangle represents the loci of Herbig Ae/Be stars (Hernández et al. 2005). In both diagrams the dashed curve represents the colours of Main Sequence stars, while the dashed-dotted line indicates the locus of classical T Tauri stars (Meyer, Calvet & Hillenbrand 1997). The reddening vector is also indicated.

The dereddened SEDs were derived for 30 of the 35 objects with spectroscopy and  $H\alpha$  in emission; the other five objects lack enough photometric measurements. Since we do not have  $U$ -band photometry, an intrinsic  $U$  magnitude was derived from the de-reddened  $B$  magnitude and the intrinsic  $(U - B)_0$  colour of the corresponding spectral type.

To further investigate excess emission in the infrared, and thus the presence of a circumstellar disk and/or of an envelope, we compared the derived SEDs with those of normal photospheres of the same spectral type. This is shown in Fig. 7 for the PMS stars only, where the black dots and dotted lines represent the SEDs of the object investigated and of normal photospheres, respectively; the error bars were computed taking into account an error of one spectral subclass. Note that the target and standard star fluxes were normalized at  $R$ -band flux. An inspection of the figures clearly reveals the stars with IR excess.

### 3.4 Luminosities

The total luminosity for each object was computed in two ways as follows. First, by integrating the de-reddened SEDs, using a cubic-spline fit to the observed  $\lambda F_\lambda$  vs  $\log \lambda$  distribution assuming isotropic radiation and the distance of 4.0 Kpc. The integration of the SEDs was carried out in the interval from  $\lambda_B$  to  $\lambda_{end}$ , the terminal wavelength ( $\lambda_K$ ,  $\lambda_L$  or  $\lambda_M$ , depending on the available IR photometric data). In order to determine the contribution of the flux downward of  $\lambda_{end}$ , we extrapolated the de-reddened flux distribution with a black-body tail, following the method by Cohen (1973).

The typical errors in  $\log L_{int}$  were estimated to be less than about 0.06 dex. Second, the  $V$  magnitude corrected for interstellar extinction was used to obtain the bolometric luminosity ( $L_{BC}$ ), by adopting a bolometric correction appropriate to a main-sequence star of the same spectral type. The relations given by Kenyon & Hartmann (1995) were used to compute the bolometric corrections.

The difference between the luminosity derived from the integration of the SED and that determined from bolometric corrections can be attributed to the excess luminosity of the circumstellar disk. For a flat, optically-thick disk, which merely reprocesses light from the star, the  $L_{disk}/L_{star}$  ratio is 0.25 (e.g. Allers et al. 2006). Such value is consistent with the results of recent Spitzer investigations of nearby star forming regions (e.g. Harvey et al. 2007; Alcalá et al. 2008). The distribution of the disk-to-star luminosity for the PMS stars identified in this work is displayed in Fig. 8. The histogram peaks at around  $\log(L_{disk}/L_{star}) = -0.35$ , i.e. at a disk luminosity which is about half the stellar luminosity and a factor of about 2 higher than what found in previous studies of nearby star forming regions. Since the cluster is about an order of magnitude more distant than the nearby star forming regions, this result reflects the fact that our spectroscopic survey revealed the most luminous disks in the Sh 2-284 complex. A detailed study of the disk parameters around the PMS stars in this region is beyond the scope of the paper, and is deferred to a future work.

The luminosity,  $\log L_{BC}$ , derived by adopting a bolometric correction should be the best approximation to the photospheric stellar luminosity. In the absence of IR excess



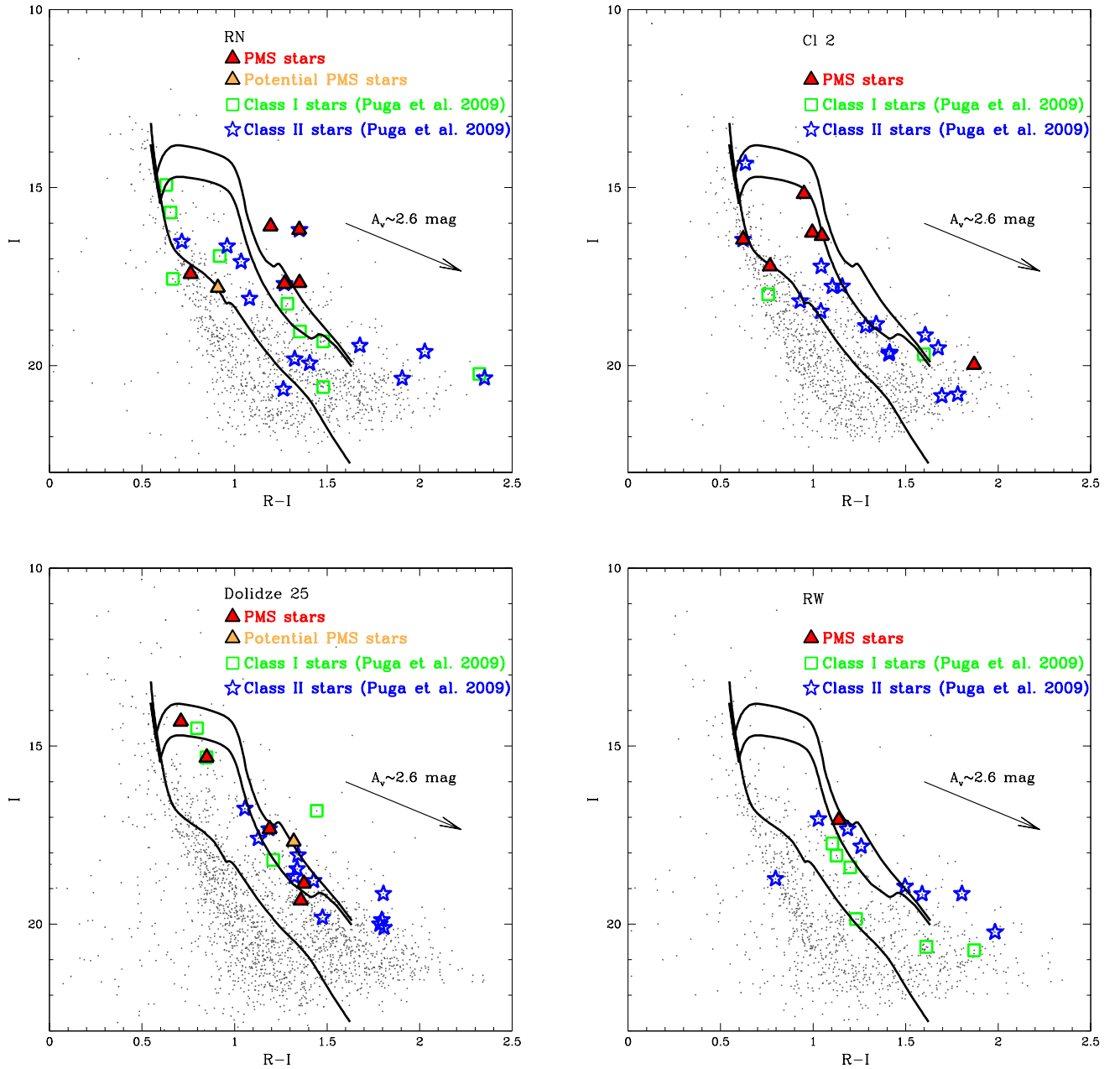


**Figure 5.**  $I$  vs.  $R - I$  diagrams of four regions in Sh 2-284, each covering approximately the same area of  $\sim 40\text{arcmin}^2$  in the sky. The regions correspond to RN, Cl2, Dolidze 25, and RW, as designated by P09. The 1,2 and 20 Myr isochrones, with metallicity  $Z=0.004$  by Tognelli et al. (2010), are represented with solid lines. The Tognelli et al. (2010) isochrones were computed for masses in the range  $0.2-7 M_{\odot}$ . Both isochrones were reddened by the average value  $A_V = 2.6$  mag and shifted by the distance modulus 13.0 mag.

$\log L_{\text{BC}}$  should be consistent with  $\log L_{\text{int}}$ . We have confirmed that for the objects without significant IR excess  $\log L_{\text{int}} - \log L_{\text{BC}} < 0.04$  dex, which is well within the mean error estimated for  $\log L_{\text{int}}$ . We thus use the luminosities derived by adopting a bolometric correction for the subsequent analysis. Such values are reported in Table 4.

### 3.5 Masses and ages

Using the derived effective temperatures and bolometric luminosities it is possible to estimate the masses and ages of the PMS stars by comparison with PMS evolutionary tracks and isochrones on the HR diagram. To this aim we adopted the evolutionary tracks and isochrones by Tognelli et al. (2010) which are computed for the right metallicity of the Sh 2-284 star forming region and that include up-to-date input physics.

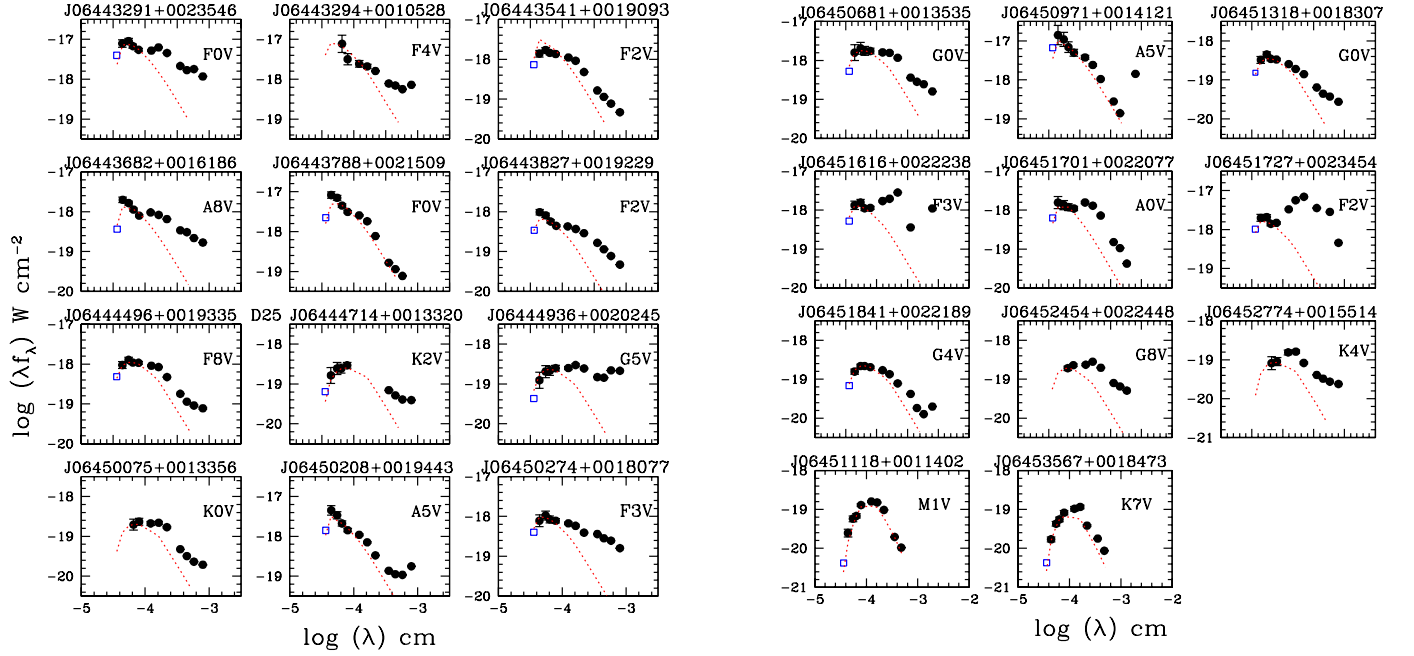


**Figure 7.** Spectral energy distribution of PMS stars in Sh 2-284. The dots represent the dereddened flux at each band. The dashed lines represent the SED of normal photospheres of the same spectral type as the object. The blue open squares represent the flux in the U band, calculated from the B magnitude as explained in the text. On the bottom right the SED for the two potential PMS are plotted.

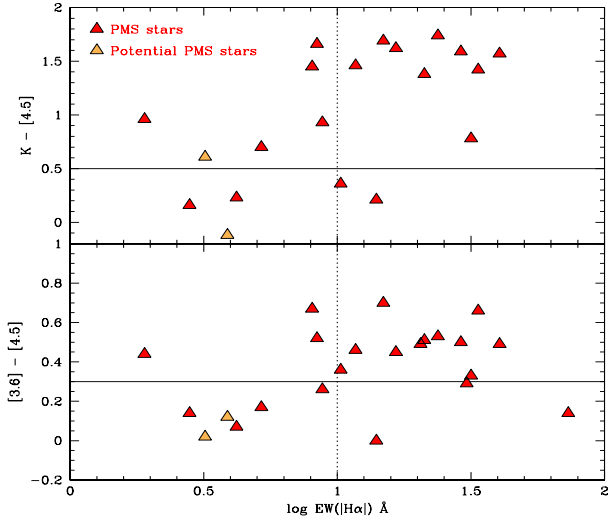


**Figure 6.** IR colours versus the strength of the  $H\alpha$  emission of the PMS stars in Sh 2-284. The upper panel shows the  $K - [4.5]$  colour v.s.  $EW_{H\alpha}$  plot, while the lower one the  $[3.6] - [4.5]$  colour v.s.  $EW_{H\alpha}$  plot. The horizontal lines in each panel represent the minimum limit for IR-excess objects according to Robitaille et al. (2006), i.e.  $K - [4.5] > 0.5$  and  $[3.6] - [4.5] > 0.3$  mag, for the upper and lower panels respectively.

The HR diagram for the PMS stars in Sh 2-284 is shown in Fig. 9 where the  $Z=0.004$  tracks and isochrones are overplotted. The derived masses and ages are reported in Table 4. Here, the error in mass is half the separation between

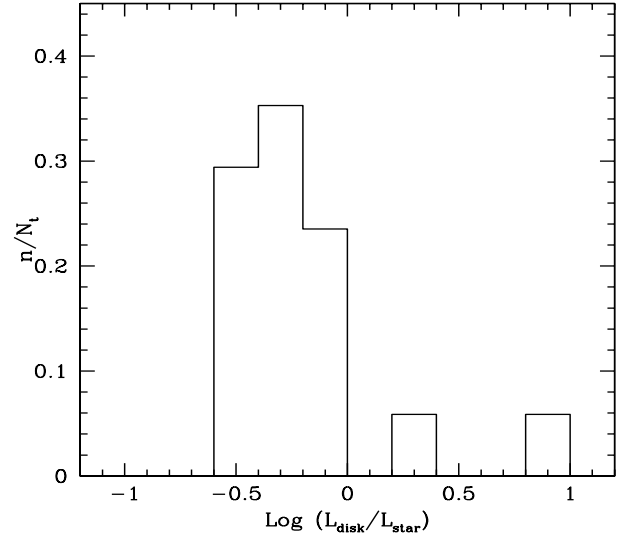


**Figure 8.** Distribution of the disk-to-photospheric luminosity ratio of PMS stars in Sh 2-284.

two consecutive evolutionary tracks. The error on the age determination is half the separation between two consecutive isochrones.

The mass of the confirmed PMS stars identified in this work ranges from 0.7 to 2.6  $M_{\odot}$ , while the age from 1.5 to 13 Myr. The lower limit for the mass is imposed by the limiting magnitude of our spectroscopic survey, but should the potential PMS candidates be confirmed, this limit would

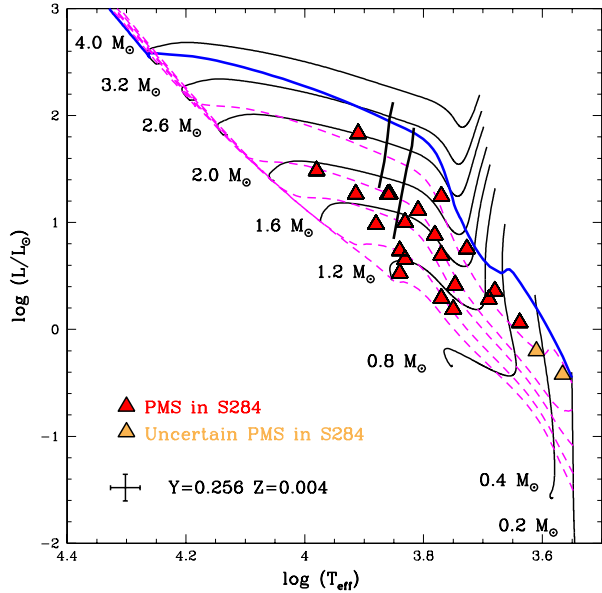


**Figure 9.** HR diagram of the PMS stars in Sh 2-284. The position of the two potential PMS stars is also shown in the diagram. The PMS evolutionary tracks, ranging from  $0.2 M_{\odot}$  to  $4 M_{\odot}$  (Tognelli et al. 2010), were computed for the appropriate cluster metallicity  $Z=0.004$ . The 1 Myr isochrones is represented with the continuous thick line, while the 2, 4, 6, 10 and 15 Myr isochrones are plotted as dashed lines. The instability strip is also indicated with the two thick, almost vertical, black lines.

drop to about  $0.3 M_{\odot}$ . The age-spread may be explained in terms of different star formation episodes, most likely related to triggered star formation in the region (P09). Interestingly, most of the PMS stars very well tracing the 2 Myr isochrone (represented by solid lines in Fig. 9), lie on the field of Dolidze 25. Noteworthy, the position on the HR diagram of the two potential PMS stars (see Section 3.1) match quite precisely the 2 Myr isochrone. One of these –the M1-type star– lies also on the field of Dolidze 25, while the other one –the K7-type star– is located to the north of the cluster, in region RN by P09. Table 4 summarizes the spatial distribution of the PMS in the Sh 2-284 region.

All this shows that the PMS stars in the field of Dolidze 25 have an average age of  $\sim 1$ -2 Myr with a very small dispersion, and are indeed younger than the PMS stars in the other aggregates of Sh 2-284, as previously inferred by the optical CM diagrams of Fig. 5 and in agreement with the results by P09, based on the relative number of Class I-to-Class II sources in the different regions.

### 3.6 Candidates to PMS $\delta$ -Scuti pulsators

The PMS  $\delta$ -Scuti candidates were selected based on the position of the PMS stars relative to the instability strip. To this aim, we overplot the strip by Breger & Pamyatnykh (1998) on the HR diagram (c.f. Fig. 9). Eight stars fall, within the errors, in the instability strip. These objects are flagged in Table 4. Four of them satisfy the Herbig AeBe criterium by Hernández et al. (2005) in the near-IR colour-colour diagram. These candidates will be the subject of a follow-

up study by means of time-series photometry to confirm whether or not they are indeed pulsating stars and in that case, to derive their pulsational properties (frequencies of oscillations). These data can be compared with the predictions of non-radial pulsational models by using asteroseismical techniques to estimate independently stellar fundamental parameters such as luminosity, effective temperature and mass, as well as the distance of the host star forming region.

## 4 DISCUSSION

### 4.1 Structure and triggered star formation

The HII in Sh 2-284, with a radius of about 13.5 pc, is powered by the high-mass star population in Dolidze 25 (presumably the oldest cluster in the region) and in particular by the O9 type star. P09 define the boundaries of this HII region as “bubble B1”. The other two clusters detected with IRAC/SPITZER on the boundaries of B1, namely C12 to the north-west of Dolidze 25 and C13 to the south-east, power the two compact HII regions B2 and B3 with radii of about 1.5 pc and 2.7 pc, respectively. Other rimmed and cometary clouds in the inner regions of B1 have been clearly detected in the IRAC/SPITZER images containing a number of YSO candidates; in particular, the “tail” of RW apparently points away from Dolidze 25 and contains a number of Class I sources. Such hierarchical structure and the spatial distribution of the different IR-class YSO candidates, indicate that star formation has occurred in the different places of the HII region over a few Myr.

As demonstrated in this work, Sh 2-284 is not only a site of high-mass star formation, but its population also comprises very young intermediate and low-mass stars, similarly as in other star forming complexes in which triggered star formation is in act, like in the Orion OB association.

Spectroscopic surveys in the optical are generally biased towards the detection of Class II and Class III sources rather than to Class I sources. The photometric properties of the Class I and Class II YSO candidates drawn from the IRAC/Spitzer observations are very similar to those of the spectroscopically confirmed PMS stars. Therefore, although there may be some extragalactic contaminants specially among the Class I sources, we can safely conclude that the sample of YSO candidates represents well the population of young stellar objects in Sh 2-284 and can be used to trace the star formation in the region.

As concluded from the optical colour-magnitude diagrams, different aggregates seem to trace different star formation episodes. In fact, from the relative numbers of Class I to Class II objects, P09 determined that the YSOs projected on the field of Dolidze 25 are younger than those projected on the other aggregates in C12 and C13. Despite our low-number statistics, the PMS stars projected on the field of Dolidze 25 appear sharply coeval both, on the HR diagram and in the optical colour-magnitude diagram. More importantly, such stars are also significantly younger than the stars in the other aggregates, in line with the P09 conclusions. Noteworthy, the IRAC YSO candidates on the field of Dolidze 25 also show a very low dispersion along the 2 Myr isochrone on the  $I$  vs.  $R - I$  diagram (see Figure 5). These facts seem to support indeed the idea of a possible alignment

of very young stars in the line of sight, which are located on the near-side of the B1 shell, as suggested by P09 and Delgado et al. (2010). In addition, the high relative number of Class I sources (158) with respect to Class II sources (188) in Sh 2-284, points towards a non-continuous star formation in the region. We thus conclude that star formation on the B1 shell was most likely triggered by the impact of the massive stars of Dolidze 25, leading first to the formation of the stars in clusters Cl2 and Cl3 and then to the stars on the near-side of B1. The size of the two compact HII regions B2 and B3, and the age-spread of the PMS stars in the other aggregates suggests that the Cl2 and Cl3 formed some 2 Myr before the youngest PMS stars appeared on the birth-line.

Delgado et al. (2010) predict two populations of different age in Dolidze 25, one  $\sim 4$  Myr old and the other with an average age of 40 Myr, but the presence of the O9-type star in Dolidze 25, implies that the cluster should be younger than  $\sim 20$  Myr. With some assumptions on the recombination coefficient, isothermal sound speed and electronic density P09 estimated dynamical ages of  $< 3.8$  Myr and  $< 1.8$  Myr for the HII regions B1 and B2, respectively. Considering an age of  $\sim 5$  Myr for Dolidze 25 and by comparison with the youngest dynamical estimate, an age-spread of the order of 3 to 4 Myr would be expected for the region. However, the low-metallicity of the region may influence the recombination coefficient, isothermal sound speed and electronic density, with an important impact on determinations of the dynamical ages. The age-spread derived from our HR diagram is  $< 10$  Myr. In addition, although our number statistic is low, we do not find strong evidence of a low-mass star population as old as 40 Myr.

In summary, the first generation of stars in the Sh 2-284 region was formed in a cluster some 10 Myr ago. The strong UV radiation and winds of the massive stars swept up the interstellar matter surrounding the cluster, triggering the formation of the stars associated with Dolidze 25. Then, the massive stars of the latter excited the HII region Sh2-284 which in turn prompted the formation of other structures, such as the Cl2 and Cl3 clusters.

Then the youngest generation of stars and rimmed clouds, with their young clusters and aggregates that we see today in the IRAC/Spitzer images, were formed about 2 Myr ago. Many Class I and Class II YSOs in the region should belong to this latter generation, but many older YSOs of previous generations may have preserve their disks/envelopes.

## 4.2 Survival of disks/envelopes

Metallicity may play an important role on circumstellar disk/envelope evolution. In a recent study of the young (age  $\sim 1$  Myr) stellar populations in low-metallicity regions of the galaxy, Yasui et al. (2009) find that the disk fraction is significantly lower than in star forming regions of solar-metallicity. They suggest that the low-metallicity may induce an increase of the mass accretion rate and/or a very efficient photo-evaporation of the circumstellar matter, both processes leading to a very rapid disk dispersal. As a consequence most stars forming in a low-metallicity environment should experience the disk dispersal at an earlier stage ( $< 1$  Myr) than those forming in a solar metallicity environment ( $\sim 5-6$  Myr). Other studies of candidates to low-mass PMS stars in the LMC (Spezzi et al. 2010) also suggest a

higher mass accretion-rate, by up to an order of magnitude, in comparison with the values derived for their Galactic counterparts.

Because of the low-metallicity environment in Sh 2-284, a low fraction of disks/envelope systems among the oldest YSOs is expected. Yet, the large number of Class I and Class II YSO candidates detected in Sh 2-284 and the age spread of more than 4 Myr indicate that a significant fraction of YSOs may have preserved their circumstellar disks/envelope, unless they represent the youngest generation. Indeed, the YSO candidates were selected based on their red IRAC colours and the sample might be biased towards the youngest IR-excess objects.

Our VIMOS spectroscopic survey was designed to include not only IR-excess YSO candidates, but also PMS candidates that may or may not have IR excess. The VIMOS sample is thus unbiased towards IR excess and hence, can be used to investigate how many of the oldest PMS stars have eventually preserved their disks. Of the 23 PMS stars, there are 16 (i.e.  $\sim 70\%$ ) with an age  $t \geq 3$  Myr. Of these, 10 possess strong IR-excess, indicative of an optically thick circumstellar accretion disk (see Fig. 7). Likewise, from Figure 6 we find that 7 out of 13 objects with  $t \geq 3$  Myr show strong IR-excess and hence, should possess an optically thick disk according to the IR-colour criterium by Robitaille et al. (2006). These results would also indicate that a significant fraction of the oldest PMS stars in Sh 2-284 have preserved their accretion disks, despite the low-metallicity environment. The number statistics of our sample is low, but should this result be confirmed with further spectroscopic observations, it will imply that disk survival may not only depend on metallicity, but also on other environmental physical conditions and/or the properties of the central objects.

Assuming that all Class II sources eventually evolve into Class III sources when their disks are fully accreted by the PMS stars, Bertout et al. (2007) estimated that the disk lifetimes for the Taurus-Auriga PMS population should be given by  $t_{disk} = 4 \times (M_*/M_\odot)^{0.75}$  Myr. This means that the disk of a  $0.5 M_\odot$  Taurus-Auriga star survives  $\sim 2$  Myr, on the average. Though applicable to solar metallicity stars, such relationship would imply an average disk-lifetime of the order of 5.5 Myr for the average  $\sim 1.5 M_\odot$  star in our PMS sample, i.e. rather consistent with the average age of 5.3 Myr drawn from the HR diagram. However, our sample is not complete specially in the low-mass regime and hence, may be biased towards massive PMS stars. In addition, the relationship by Bertout et al. (2007) was derived for young stars with masses sensibly lower than those in Sh-2-284. Hence, these results should be taken with care. In any case, a complete spectroscopic survey of the region, down to about  $0.3 M_\odot$ , is crucial to investigate the disk survival in the region. This calls for a more complete spectroscopic survey.

## 5 CONCLUSIONS

Through VIMOS@VLT, 2MASS and Spitzer data we have investigated the low-metallicity star forming region Sh 2-284. On the basis of H $\alpha$  emission, IR excess, as well as of IR colour-magnitude and colour-colour diagrams, we identified 23 new PMS stars in the region. We have character-

ized the star sample by determining the PMS stellar physical parameters. The IR properties of these stars and the Spitzer/IRAC selected YSO candidates by P09 are similar in many respects, but the latter sample is biased towards IR-excess objects.

By detailed spectroscopic parallax of three OB stars in the region we have estimated a distance of 4 Kpc for Sh 2-284.

The PMS stars found in the field of view of Dolidze 25 have an average age of 2 Myr, i.e. younger than the objects in the other aggregates of the region, in agreement with the results from the number ratio of Class I-to-Class II sources by P09 throughout the region. The age spread of the PMS, their spatial distribution and the cloud structure of Sh 2-284 suggest a sequence of star formation events, hence, that triggered star formation is in act in the region, with the massive stars of Dolidze 25 being the main triggers of the B1 shell. All this supports the idea of a possible alignment of the very young stars in the line of sight, which are located on the near-side of the B1 shell, as suggested by P09 and Delgado et al. (2010).

Despite the low-metallicity environment, a significant fraction of the oldest PMS stars in Sh 2-284 have preserved their accretion disks/envelopes. Although this result may be affected by the poor statistics of our spectroscopic sample, the large number of Class I and Class II sources in the different aggregates and their apparent age spread in the colour-magnitude diagrams seems to support it.

Among the 23 discovered young stars in Sh 2-284, we selected 8 with intermediate mass that are very good candidates for PMS  $\delta$  Scuti type pulsation. These stars will be studied with asteroseismological techniques from the ground.

## ACKNOWLEDGMENTS

We are grateful to the referee Prof. W. Lawson for his useful comments and suggestions. This work was supported by the Italian ESS project, contract ASI/INAF I/015/07/0, WP 03170 and by the European Helio- and Asteroseismology Network (HELAS), a major international collaboration funded by the European Commission's Sixth Framework Programme. EP is funded by the Spanish MICINN under the Consolider-Ingenio 2010 Program grant: First Science with the GTC. This research has made use of the SIMBAD database, operated at CDS, Strasbourg, France. This publication makes use of data products from the Two Micron All Sky Survey, which is a joint project of the University of Massachusetts and the Infrared Processing and Analysis Center/California Institute of Technology, funded by the National Aeronautics and Space Administration and the National Science Foundation.

## REFERENCES

Alcalá J.M., Radovich M., Silvotti R. et al 2002, SPIE 4836, 406  
 Alcalá J.M., Spezzi L., Chapman N., et al. 2008, ApJ, 676, 427

Allers K.N., Kessler-Silacci J.E., Cieza L.A., & Jaffe D.T., 2006, ApJ 644, 364  
 Avedisova V. S., Kondratenko G. I. 1984, NInfo, 56, 59  
 Bertout C., Siess L., Cabrit S. 2007, A&A, 473L, 21  
 Bessell M. S. 1979, PASP, 91, 589  
 Böhm T., Zima W., Catala C., Alecian E., Pollard K., Wright D. 2009, A&A, 497, 183  
 Breger Michel 1972, ApJ, 176, 373  
 Breger M., Pamyatnykh A.A. 1998, A&A, 332, 958  
 Cardelli Jason A., Clayton Geoffrey C., Mathis John S. 1989, ApJ, 345, 245  
 Cohen M. 1973, MNRAS, 164, 395  
 Cutri R. M., Skrutskie M. F., van Dyk S. et al , 2003, tmc book  
 Delgado Antonio J., Djupvik Anlaug A., Alfaro Emilio J. 2010, A&A, 509A, 104  
 Evans N. J., Allen L. E., Blake G. A., et al. 2003, PASP, 115, 965  
 Evans N. J., Dunham M. M., Jorgensen J. K., et al. 2009, ApJS, 181, 321  
 Fazio G. G., Hora J. L., Allen L. E. et al. 2004, ApJS, 154, 10  
 Fitzsimmons A., Dufton P. L., Rolleston W. R. J. 1992, MNRAS, 259, 489  
 Flaherty K. M., Pipher J. L., Megeath S. T., et al. 2007, ApJ, 663, 1069  
 Frasca A., Alcalá J. M., Covino E., Catalano S., Marilli E., Paladino R. 2003, A&A, 405, 149  
 Gandolfi Davide, Alcal Juan M., Leccia Silvio et al. 2008, ApJ, 687, 1303  
 Hartmann L. 1998, *Accretion Processes in Star Formation* (Cambridge: Cambridge Univ. Press)  
 Hartmann L., Megeath S.T., Allen L.E., et al. 2005, ApJ 629, 881  
 Harvey P., Merín B., Huard T.L., et al. 2007, ApJ, 663, 1149  
 Hernández J., Calvet N., Briceño C., Hartmann L., Berlind P. 2004, AJ, 127, 1682  
 Hernández J., Calvet N., Hartmann L., Briceño C., Sicilia-Aguilar A., Berlind P. 2005, AJ, 129, 856  
 Kenyon S. J. & Hartmann L. 1995, ApJS, 101, 117  
 Kurucz R. L. 1979, ApJS, 40, 1  
 Lada C.J. 1987, IAUS, 115, 1  
 Lada C.J., Muench A.A., Luhman K.L., et al. 2006, AJ 131, 1574  
 LeFevre Oliver, Saisse Michel, Mancini Dario, Brau-Nogue Sylvie, Caputi Oreste et al. 2003, SPIE, 4841, 1670  
 Landolt Arlo U. 1992, AJ, 104, 340  
 Lennon D. J., Dufton P. L., Fitzsimmons A., Gehren T., Nissen P. E. 1990, A&A, 240, 349  
 Marconi M., Palla F. 1998, ApJ, 507, 141  
 Marigo P., Girardi L., Bressan A., Groenewegen M. A. T., Silva L., Granato G. L. 2008, A&A, 482, 883  
 Martin N. F., Ibata R. A., Bellazzini M., Irwin M. J., Lewis G. F., Dehnen W. 2004, MNRAS, 348, 12  
 Megeath S. T., Allen L. E., Gutermuth R. A., Pipher J. L., Myers P. C., Calvet N., Hartmann L., Muzerolle J., Fazio G. G. 2004, ApJS, 154, 367  
 Meunier J. C., Granet Y., Agneray F., Deleuil M., Surace C., Moutou C. 2009, ASPC, 411, 454  
 Meyer M. R., Calvet N., Hillenbrand L. A. 1997, AJ, 114, 288



**Table 4.** Summary of spectroscopic information and physical parameters for PMS stars. The errors on the visual extinction are in average of a tenth percent using the extinction law given in Cardelli et al. (1989). The error on the temperature comes from the one spectral sub-class uncertainty on spectral classification. The error in luminosity is dominated by the uncertainty in distance, which is of the order of 10 %. For each star we assumed a distance of 4.0 Kpc. The error in mass and age is half the separation between two consecutive tracks and isochrones, respectively. In the last column some notes are given.

id	SpT	EW(H $\alpha$ ) [Å]	EW(Ca I+ Fe I) [Å]	EW(Na I) [Å]	A <sub>v</sub> (mag)	log T <sub>eff</sub>	log L <sub>BC</sub> /L <sub>⊙</sub>	Mass (M <sub>⊙</sub> )	age (Myr)	Notes
J06443291+0023546	F0V	-23.80 ± 0.40	1.40±0.10	3.30±0.20	3.10	3.860	1.27	1.8	4.0	1, 3
J06443294+0010528	F4V	-139.28 ± 1.23	noise	1.70±0.23	3.64	3.809	1.11	1.6	4.0	1, 3, 7
J06443541+0019093	F2V	-4.20 ± 0.20	1.45±0.05	2.70±0.15	3.00	3.831	1.00	1.6	6.0	1, 5
J06443682+0016186	A8V	-8.40 ± 0.20	0.00±0.12	2.32±0.20	1.90	3.880	0.98	1.4	8.0	1, 2
J06443788+0021509	F0V	-2.80 ± 0.10	0.70±0.10	2.25±0.10	2.28	3.857	1.27	1.8	4.0	1, 5
J06443827+0019229	F2V	-11.70 ± 0.25	0.06±0.02	1.60±0.10	1.30	3.831	0.66	1.2	10.0	3, 5
J06444496+0019335	F8V	-8.80 ± 0.15	1.48±0.05	2.12±0.20	2.52	3.781	0.88	1.6	4.0	5
D25 J06444602+0019182	G0V	-73.20 ± 0.90	noise	noise	5.63	3.770	0.70	1.6	5.0	5
D25 J06444714+0013320	K2V	-20.50 ± 0.50	3.70±0.20	3.60±0.20	2.15	3.680	0.36	1.0	1.5	3, 4
J06444936+0020245	G5V	-14.87 ± 0.30	2.62±0.10	3.50±0.20	1.70	3.747	0.42	1.2	5.0	5
J06450075+0013356	K0V	-31.69 ± 0.50	-	3.54±0.30	1.89	3.690	0.28	1.2	2.0	4
J06450208+0019443	A5V	-8.05 ± 0.10	0.56±0.05	1.95±0.15	2.44	3.914	1.27	1.8	5.0	2
J06450274+0018077	F3V	-33.70 ± 0.25	1.30±0.15	2.50±0.23	3.14	3.840	0.74	1.2	10.0	1, 3
J06450681+0013535	G0V	-1.90 ± 0.10	0.00±0.20	2.00±0.10	2.00	3.770	1.25	2.3	1.5	2, 4
J06450971+0014121*	A5V	-14.00 ± 0.20	-	2.30 ± 0.30	2.11	3.910	1.83	2.6	2.0	4
J06451318+0018307	G0V	-40.50 ± 0.50	-	3.40±0.20	2.64	3.770	0.29	1.0	10.0	3
J06451616+0022238	F3V	-5.30 ± 0.25	0.35±0.10	3.17±0.30	3.01	3.840	0.53	1.2	12.5	1, 6
J06451701+0022077	A0V	-10.30 ± 0.40	0.00±0.10	1.56±0.20	3.82	3.980	1.48	2.0	4.0	6
J06451727+0023454	F2V	-16.58 ± 0.30	0.31±0.06	2.30±0.20	2.69	3.831	1.00	1.6	6.0	1, 3, 6
J06451841+0022189	G4V	-5.20 ± 0.30	2.05±0.10	2.70±0.05	1.05	3.750	0.19	1.0	10.0	6
J06452454+0022448	G8V	-21.18 ± 0.25	2.20±0.30	-	2.33	3.727	0.75	1.8	1.5	6
D25 J06452476+0013360	-	-30.50 ± 0.30	-	-	-	-	-	-	-	4
J06452774+0015514	K4V	-29.00 ± 1.30	-	-	2.77	3.638	0.06	0.7	1.5	2
J06451118+0011402	M1V	-3.88 ± 0.12	noise	7.40±0.34	0.17	3.566	-0.42	0.3	2.0	Potential PMS, 4
J06453567+0018473	K7V	-3.20 ± 0.05	2.79±0.10	6.00±0.15	0.21	3.610	-0.20	0.4	2.0	Potential PMS, 6

\*For this star we obtained a spectrum with the BFOSC instrument at the 1.5 m Tel. at the Loiano Observatory (<http://www.bo.astro.it/loiano/index.htm>), using grism #4 with an exposure of 20 minutes.

<sup>1</sup> PMS  $\delta$  Scuti candidates.

<sup>2</sup> Object matching Class I source in P09.

<sup>3</sup> Object matching Class II source in P09.

<sup>4</sup> Star member of Dolidze 25.

<sup>5</sup> Star member of Cl2 (see definition in P09).

<sup>6</sup> Star member of RN (see definition in P09).

<sup>7</sup> Star member of RW (see definition in P09).

**Table 5.** Physical parameters of Field stars with emission in the H $\alpha$  line. Columns are the same as in Table 3.

id	SpT	EW(H $\alpha$ ) [Å]	EW(Ca I+ Fe I) [Å]	EW(Na I) [Å]	A <sub>v</sub> (mag)	log T <sub>eff</sub>	log L <sub>BC</sub> /L <sub>⊙</sub>	Mass (M <sub>⊙</sub> )	age (Myr)	Notes
J06445227+0014300	M2.5V	-5.10 ± 0.23	2.39±0.13	10.00±0.67	0.00	3.519	-	-	-	Dme
J06445433+0021190	M4.5V	-20.71 ± 0.34	1.22±0.40	3.20±0.34	0.36	3.482	-	-	-	Dme
J06450151+0008493	M2.5V	-7.20 ± 0.10	1.15±0.30	5.25±0.20	0.00	3.547	-	-	-	Dme
D25 06452246+0015408	M4V	-8.22 ± 0.23	noise	noise	0.00	3.510	-	-	-	Dme
J06453429+0022261	M2V	-1.58 ± 0.23	2.37±0.21	8.79±0.23	0.00	3.510	-	-	-	Dme
J06453550+0024158	M2V	-11.90 ± 0.25	-	9.00±0.20	1.29	3.550	-	-	-	Dme
J06453643+0011254	M3.5V	-3.90 ± 0.23	2.54±0.20	8.95±0.40	0.00	3.506	-	-	-	Dme
D25 J06454297+0011461	M4V	-9.15 ± 0.15	3.89±0.40	4.01±0.80	0.00	3.510	-	-	-	Dme
J06454948+0011347	M4V	-0.18 ± 0.10	-	-	0.00	3.493	-	-	-	Dme
J06455486+0008134	M2V	-8.50 ± 0.20	-	2.89±0.20	0.52	3.550	-	-	-	Dme

M. et al. 2004, ApJS, 154, 1

Yasui Chikako, Kobayashi Naoto, Tokunaga Alan T., Saito

Masao, Tokoku Chihiro 2009, ApJ, 705, 54